Journal of Catalysis 257 (2008) 369–381

Contents lists available at ScienceDirect

Journal of Catalysis

www.elsevier.com/locate/jcat

Effect of the addition of Au in zirconia and ceria supported Pd catalysts for the direct synthesis of hydrogen peroxide

Federica Menegazzo [a], Pierluigi Burti [a], Michela Signoretto [a], Maela Manzoli [b], Svetoslava Vankova [b], Flora Boccuzzi [b], Francesco Pinna [a], Giorgio Strukul [a,*]

[a] Dipartimento di Chimica, Università di Venezia, and Consorzio INSTM, 30123 Venezia, Italy
[b] Dipartimento di Chimica IFM and NIS Centre of Excellence, Università di Torino, 10125 Torino, Italy

ARTICLE INFO

Article history:
Received 13 March 2008
Revised 15 May 2008
Accepted 15 May 2008
Available online 16 June 2008

Keywords:
Hydrogen peroxide direct synthesis
Palladium
Gold
Sulfated zirconia
Sulfated ceria
Reactivity
HRTEM
FTIR
Mechanism

ABSTRACT

Mono- and bimetallic palladium–gold catalysts supported on zirconia and ceria, both sulfated and non-sulfated, are tested for the direct synthesis of hydrogen peroxide under very mild (1 bar and 20 °C) and non-explosive conditions. Catalysts are characterized by N_2 physisorption, sulfur content analysis, temperature programmed reduction (TPR), Fourier transmission infrared (FTIR) spectroscopy and high resolution transmission electron microscopy (HRTEM). Catalytic tests are carried out with different gas mixtures and after various pretreatments. Best catalytic results are observed using sulfate doped zirconia samples and H_2/O_2 mixtures containing a large excess of oxygen. Monometallic gold catalysts are completely inactive, while the addition of gold to palladium improves both the productivity and the selectivity of the process. Surface oxidized Pd and Pd–Au catalysts pretreated with hydrogen and oxygen show higher activity and selectivity with respect to non-pretreated samples. A mechanistic explanation is proposed.

1. Introduction

Hydrogen peroxide has always been considered a very interesting and environmentally friendly oxidant with applications confined mainly in unselective sectors such as the paper and textile industry and the treatment of waste waters. More recent applications in the chemical industry are related to the discovery of TS-1 molecular sieve and its ability to promote large scale selective oxidation processes such as the epoxidation of olefins, the hydroxylation of aromatics, and the synthesis of cyclohexanone oxime, a key intermediate in the production of nylon-6 [1]. These and other possible smaller scale applications of hydrogen peroxide as oxidant would greatly benefit from on-site, moderate scale production facilities that would avoid transport costs.

The increasing demand for hydrogen peroxide [2,3] and the general need for greener oxidants is revamping the interest for a possible alternative to the auto oxidation of alkyl anthraquinone route, based on the direct combination of H_2 and O_2 [4]. The anthraquinone process, although used on a multi-million tonne scale annually, suffers from several limitations: (i) it produces a significant amount of organic waste due to the over-reduction of anthraquinone, (ii) it needs several costly separation and concentration steps, and (iii) it is economically feasible only on large scale plants. The synthesis of hydrogen peroxide by direct reaction of hydrogen and oxygen has long been an attractive alternative but has never found industrial application because of two major drawbacks. First, H_2/O_2 gas mixtures are explosive over a wide range of concentrations (4–94% H_2 in O_2), causing serious safety problems. Second, good yields and selectivities to hydrogen peroxide rather than water are very difficult to obtain, since the same catalysts used to produce H_2O_2 are also active for its decomposition and its hydrogenation to water as well as for water direct synthesis.

Several patents concerning the direct synthesis of H_2O_2 [5–10], and a number of scientific works have been published in the open literature over the last decades [11–25]. Most patents and papers deal with explosive hydrogen/oxygen mixtures and high pressures, needed to improve H_2O_2 yield. However, operating commercially in the explosion region is extremely dangerous, thus more recent studies have concentrated on carrying out the reaction with diluted H_2/O_2 mixtures well away from the explosion regime [26,27]. Until very recently, the catalysts used in these investigations were based predominantly on palladium. In the past few years, Hutchings and co-workers have reported that catalysts based on Au–Pd alloys supported on alumina [14], iron oxide [17], titanium oxide [18], or carbon [28] can significantly improve the rate of hydrogen peroxide formation when compared with the Pd only catalyst.

* Corresponding author. Fax: +39 041 234 8517.
E-mail address: strukul@unive.it (G. Strukul).

0021-9517/$ – see front matter
doi:10.1016/j.jcat.2008.05.019

However all these investigations were performed using moderately high pressures (37 bar).

The present paper reports the preparation and use of mono- and bimetallic palladium–gold catalysts for the direct synthesis of hydrogen peroxide under very mild conditions (20 °C and 1 bar) and outside the explosion range. Zirconia and ceria, both plain and sulfated, were chosen as supports. Since H_2O_2 is more stable under acidic conditions, a strongly acidic support can prove useful, in principle, for the direct synthesis of H_2O_2. It is known [29] that the surface acidity/basicity of zirconia can be controlled by addition of different dopants, SO_4^{2-} being the most investigated one. On the contrary there are almost no studies regarding sulfated ceria [30]. The latter support is characterized by a high oxygen storage capacity (OSC) and reducibility [31] and it is chosen in this work because it has been previously shown [24–26] that partially oxidized Pd seems to play an important role in the reaction.

2. Experimental

2.1. Materials

$ZrOCl_2$ (Fluka), $(NH_4)_2Ce(NO_3)_6$ (Sigma–Aldrich), $(NH_4)_2SO_4$ (Merck), were used for sample synthesis as received. All kinetic tests were performed in anhydrous methanol (SeccoSolv, Merck, $[H_2O] < 0.005\%$). Commercial standard solutions of $Na_2S_2O_3$ (Fixanal [0.01], Hydranal-solvent E, and Hydranal-titrant 2E, all from Riedel–de Haen) were used for iodometric and Karl–Fischer titrations.

2.2. Catalyst preparation

Zirconia support was prepared by precipitation from $ZrOCl_2$ at constant pH (pH 10), aged under reflux conditions [32,33], washed free from chloride ($AgNO_3$ test) and dried at 110 °C overnight. Ceria support was synthesized by precipitation from $(NH_4)_2Ce(NO_3)_6$ by urea at 100 °C in aqueous solution [34]. The solution was continuously mixed and boiled for 6 h at 100 °C, the precipitate was washed twice in boiling deionized water and dried at 110 °C overnight. These materials were impregnated by an incipient wetness method with $(NH_4)_2SO_4$ in amounts necessary to yield an 8 wt% anion loading. Impregnated supports were then calcined in flowing air (50 ml/min) at 650 °C for 3 h. Calcined supports were impregnated by incipient wetness with H_2PdCl_4 and/or $HAuCl_4$ aqueous solutions to give a nominal 2.5 wt% metal loaded catalyst and finally calcined again at 500 °C in flowing air for 3 h.

2.3. Methods

Surface areas and pore size distributions were obtained from N_2 adsorption/desorption isotherms at −196 °C (using a Micromeritics ASAP 2000 analyzer). Calcined samples (300 mg) were pretreated at 300 °C for 2 h under vacuum. The non-calcined sample was pretreated at 100 °C for 2 h under vacuum. Surface area was calculated from the N_2 adsorption isotherm by the BET equation, and pore size distribution was determined by the BJH method [35]. Total pore volume was taken at $p/p_0 = 0.99$.

The amount of sulfate was determined by ion chromatography (IEC) after dissolution of the materials [36]. All sulfate concentrations were calculated as the average of two independent sample analyses, and each analysis included two chromatographic determinations.

Metal loading was determined by atomic absorption spectroscopy after microwave disgregation of the samples (50 mg).

TPR experiments were carried out in a home-made equipment: samples (100 mg) were heated with a 10 °C/min ramp from 25 to 1200 °C in a 5% H_2/Ar reducing mixture (40 ml/min STP).

HRTEM analysis was performed on all catalysts using a Jeol 2000 EX electron microscope (200 kV) equipped with a top entry stage and a LaB_6 filament. The powdered samples were ultrasonically dispersed in isopropanol and the obtained suspension was deposited on a copper grid, coated with a porous carbon film.

FTIR spectra were taken on a Perkin–Elmer 1760 spectrometer (equipped with a MCT detector) with the samples in self-supporting pellets introduced in a cell allowing thermal treatments under controlled atmosphere. The pretreatments of samples before the spectroscopic experiments were: (i) outgassing of the untreated samples at room temperature; (ii) pretreatment at room temperature with 5 mbar of H_2; (iii) pretreatment at room temperature with 5 mbar of H_2 and 5 mbar of O_2. After these pretreatments 35 mbar of CO were admitted at room temperature. The spectrum of the sample before CO inlet was subtracted from each spectrum. All spectra were normalised to the same palladium content.

2.4. H_2O_2 synthesis

Catalytic tests were carried out at atmospheric pressure in a 20 °C thermostatted glass reactor according to a previously described procedure [26]. Mixing was carried out with a Teflon-made rotor operating at 1000 rpm. Oxygen or air, hydrogen and nitrogen were bubbled by a gas diffuser directly into the liquid phase with a total flow of 50 ml/min. Different gas feeds with the following composition were used:

- $H_2/O_2/N_2$ 10/10/80 (denoted as 10/10) (*Caution*: this is just outside the explosion range, but not outside the flammable range) [37].
- $H_2/O_2/N_2$ 4/10/86 (denoted as 4/10) (nonexplosive and nonflammable mixture) [37].
- H_2/O_2 4/96 (denoted as 4/96) (nonexplosive and lower limit for nonflammable mixture) [37].

All catalytic tests were carried out in methanol. 100 ml of a 0.03 M H_2SO_4 methanolic solution was pre-saturated with the gas mixture before catalyst (135 mg if not otherwise indicated) introduction. Catalysts were introduced neither reduced nor pre-treated before use. During catalytic tests small aliquots of the liquid phase were sampled through a septum and used for water and hydrogen peroxide determination. H_2O_2 concentration was measured by iodometric titration, whereas water was determined by volumetric Karl–Fischer method. The water content in the reaction medium before catalyst addition was determined prior to each catalytic experiment. H_2O_2 selectivity at time t was determined as follows:

$$S_{H_2O_2} = \frac{[H_2O_2]}{[H_2O_2] + [H_2O]}$$

A simple model was used to fit the kinetic data and find the apparent kinetic constants of the four reactions involved in the catalytic process (see Scheme 1). We accounted only for H_2O_2 decomposition by H_2 reduction, while H_2O_2 disproportionation reaction was not considered, as it was found to be negligible under our reaction conditions [25].

In the system of differential equations coming from mass balance (see Scheme 2) the concentrations of H_2 and O_2 into the

$$H_2 + O_2 \xrightarrow{k_1} H_2O_2$$
$$H_2 + 1/2O_2 \xrightarrow{k_2} H_2O$$
$$H_2O_2 + H_2 \xrightarrow{k_3} 2H_2O$$
$$H_2O_2 \xrightarrow{k_4} H_2O + 1/2O_2$$

Scheme 1.

$$\frac{dc_{H_2}}{dt} = -k_1 c_{H_2}^{a} c_{O_2}^{b} - k_2 c_{H_2}^{c} c_{O_2}^{d} - k_3 c_{H_2O_2} c_{H_2}^{e}$$
$$\frac{dc_{O_2}}{dt} = -k_1 c_{H_2}^{a} c_{O_2}^{b} - k_2 c_{H_2}^{c} c_{O_2}^{d}$$
$$\frac{dc_{H_2O_2}}{dt} = k_1 c_{H_2}^{a} c_{O_2}^{b} - k_3 c_{H_2O_2} c_{H_2}^{e}$$
$$\frac{dc_{H_2O}}{dt} = k_2 c_{H_2}^{c} c_{O_2}^{d} + 2k_3 c_{H_2O_2} c_{H_2}^{e}$$

Scheme 2.

Table 1
Surface features of calcined samples

Sample	SSA (m^2/g)	Pore diameter (nm)	Pore volume (cm^3/g)
Z	61	21.3	0.327
ZS	129	11.1	0.332
Ce	53	7.1	0.073
CeS	29	19.5	0.099

liquid phase can be considered constant, since these reagents are continuously fed into the semi-batch reactor. Their concentrations can be incorporated into the kinetic constants k_n to give apparent kinetic constants k'_n, and the resulting system of differential equations can be solved for the H_2O_2 and H_2O concentrations to give:

$$c_{H_2O_2} - c^0_{H_2O_2} = \frac{k'_1}{k'_3}\left(1 - e^{-k'_3 t}\right)$$

and

$$c_{H_2O} - c^0_{H_2O} = \left(k'_2 + 2k'_1 + 2k'_3 c^0_{H_2O_2}\right)t - 2\frac{k'_1}{k'_3}\left(1 - e^{-k'_3 t}\right).$$

Catalytic tests data fitting was carried out with a computer program (OriginLab OriginPro7.5), equipped with a special fitting tool (based on the Levenberg–Marquardt (LM) algorithm) performing non-linear regression analysis.

3. Results and discussion

3.1. N_2 physisorption analyses

The use of mesoporous materials is very important in this investigation, since the presence of micropores could bear mass transfer problems, while a low surface area would not allow a good dispersion of the active phase. So N_2 physisorption analyses were carried out in order to determine surface areas and pore size distributions of the supports.

The N_2 physisorption isotherms for the zirconia calcined samples are shown in Fig. 1a and data are reported in Table 1. As can be seen, whether plain or sulfated all zirconia samples display type IV isotherms with hysteresis loops typical of mesoporous materials. Plain zirconia shows a low surface area (<60 m^2/g). On the contrary, as already reported for other samples [38,39], sulfate doping yielded a material retaining a high surface area (<130 m^2/g) and a mesoporous structure with a mean pore size around 10 nm. Sulfates bind strongly avoiding or, at least, retarding structure collapse during calcination [29].

The N_2 physisorption isotherms for the ceria calcined samples are shown in Fig. 1b and data are reported in Table 1. As can be seen, also ceria samples display type IV isotherms with hysteresis loops typical of mesoporous materials. Non-calcined, non-doped ceria precursor (not shown) was also mesoporous (BJH mean pore size 5.7 nm) with a higher surface area (128 m^2/g) than the calcined samples. Both ceria supports show surface areas lower than zirconia supports. Besides, in ceria samples sulfates do not prevent

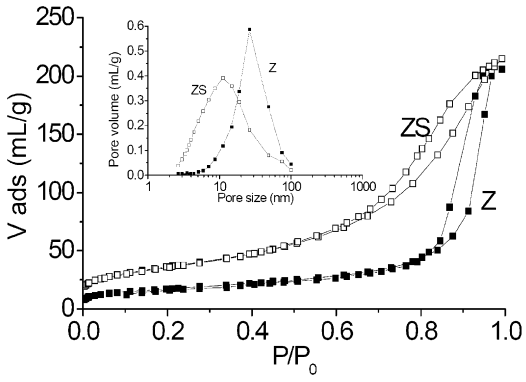

(a)

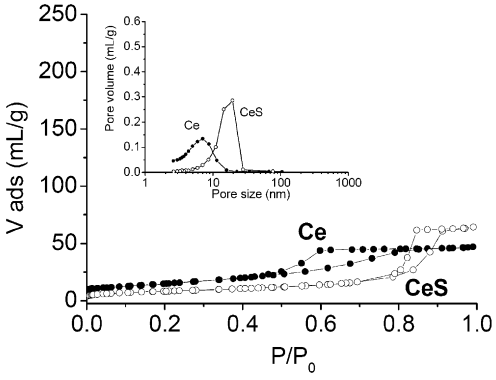

(b)

Fig. 1. N_2 physisorption isotherms of zirconia (a) and ceria (b) calcined samples and (insert) their BHJ pore size distributions.

Table 2
Metal and sulfates loading on final catalysts

Sample	Pd loaded (wt%)	Pd found (wt%)	Au loaded (wt%)	Au found (wt%)	$SO_4^{=}$ found (wt%)
Z–Pd	2.50	2.61	–	–	–
ZS–Pd	2.50	2.12	–	–	4.0
Z–Au	–	–	2.50	2.04	–
ZS–Au	–	–	2.50	1.89	4.2
Z–PdAu	1.25	1.21	1.25	0.95	–
ZS–PdAu	1.25	1.22	1.25	0.92	4.2
Ce–Pd	2.50	2.68	–	–	–
CeS–Pd	2.50	2.69	–	–	6.4
Ce–Au	–	–	2.50	2.20	–
CeS–Au	–	–	2.50	2.30	7.1
Ce–PdAu	1.25	1.24	1.25	1.10	–
CeS–PdAu	1.25	1.01	1.25	1.10	6.9

structure collapse and pore wall thickening. At variance with zirconia, the sulfated material has a very low surface area (<30 m^2/g), even lower than the plain ceria support (<50 m^2/g).

In Table 2 metal and sulfate loading on final catalysts are reported. As can be seen, all Pd theoretically loaded on samples is found in both zirconia and ceria catalysts. This confirms that incipient wetness impregnation is a preparation technique allowing almost all the desired metal be loaded in the samples. On the contrary the gold amount found in the samples after calcination is less than expected. This could be due either to impurities in the $HAuCl_4$ used in sample preparation, or to difficulties in properly analyzing gold–chlorine complexes formed during catalyst disgregation. It should be noted that samples with a Pd/Au 1/1 ratio on a weight basis correspond to 2/1 on a molar basis.

In Table 2 also the SO_4^{2-} wt% found in the catalysts after calcination is reported. All samples were impregnated with amounts necessary to yield 8 wt% anion loading. In zirconia supported catalysts the final amount of sulfates is about 4 wt%, a typical value

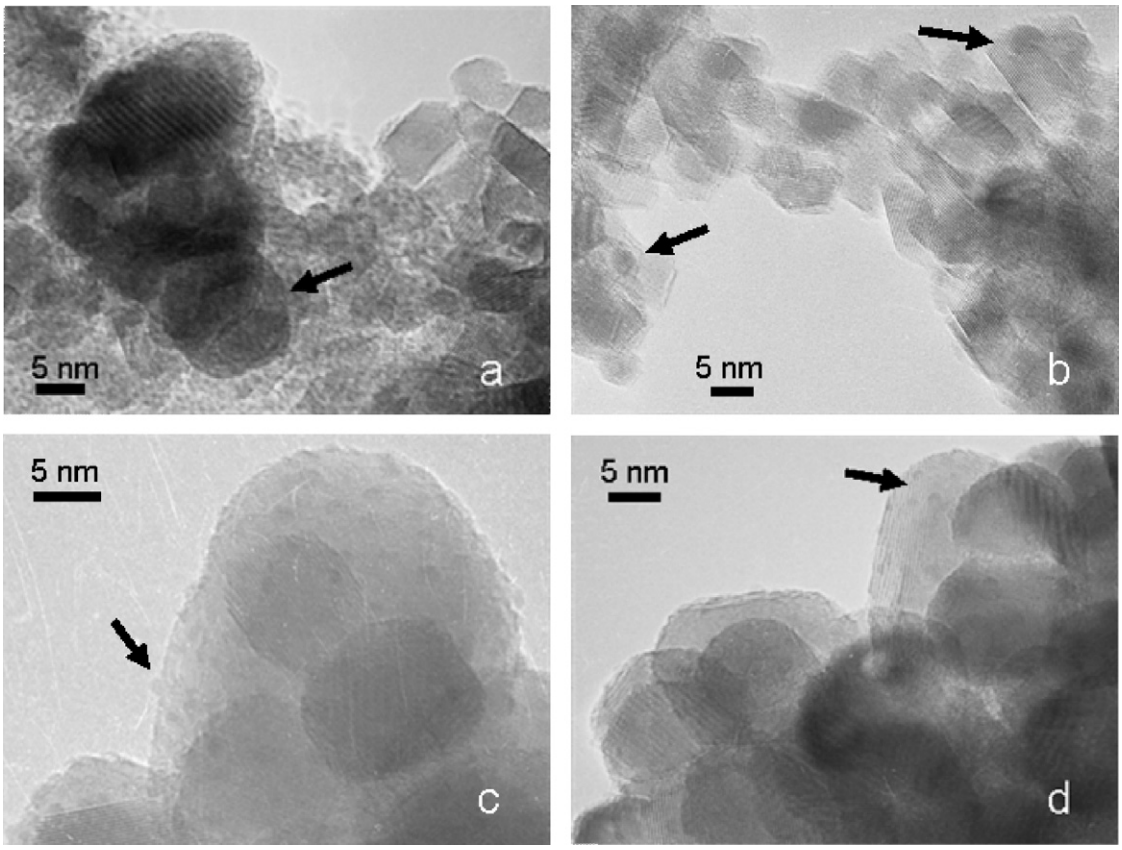

Fig. 2. HRTEM images of ZS–Pd (a), ZS–PdAu (b), CeS–Pd (c), and CeS–PdAu (d). Original instrumental magnification ×500,000.

for these catalysts after calcination at 650 °C [39]. As for ceria supported samples, the values are higher, about 7 wt%, but in this case no comparison could be found in the literature.

3.2. HRTEM characterization

The results of HRTEM analysis performed on both monometallic and bimetallic sulfated catalysts are resumed in Fig. 2 where the HRTEM images are shown and Fig. 3 where the metal particle size distribution for each sample is reported.

HRTEM measurements evidenced crystalline nanoparticles of sulfated zirconia whose size ranges between 5 and 10 nm on both mono- and bimetallic samples (Figs. 2a and 2b, respectively). Easily detectable palladium particles (evidenced by the arrow in Fig. 2a) and particles agglomerates have been observed on ZS–Pd, while in ZS–PdAu (Fig. 2b), metal particles are more difficult to observe (see arrows) since their size was lower than in the monometallic catalyst. It has to be pointed out that round shaped particles of about 100 nm, possibly of gold, have been observed in some regions of the latter sample (not shown for the sake of brevity). No evidence for small Au particles was found, although an influence for the presence of gold in proximity of palladium is quite evident from reactivity and IR data (see below).

In sulfated ceria-supported catalysts, HRTEM analysis showed round shaped crystalline ceria with dimensions in the 15–30 nm range. The larger size indicates that CeS has a smaller surface area with respect to ZS, in agreement with BET results. Moreover, very small metallic particles (evidenced by arrows) have been observed on both sulfated ceria-supported catalysts (Figs. 2c and 2d, respectively).

More detailed information on the metal particle size of all samples are given in Fig. 3. In particular, the obtained average size of the Pd particles detected on ZS–Pd is 6.4 nm (Fig. 3a). The size

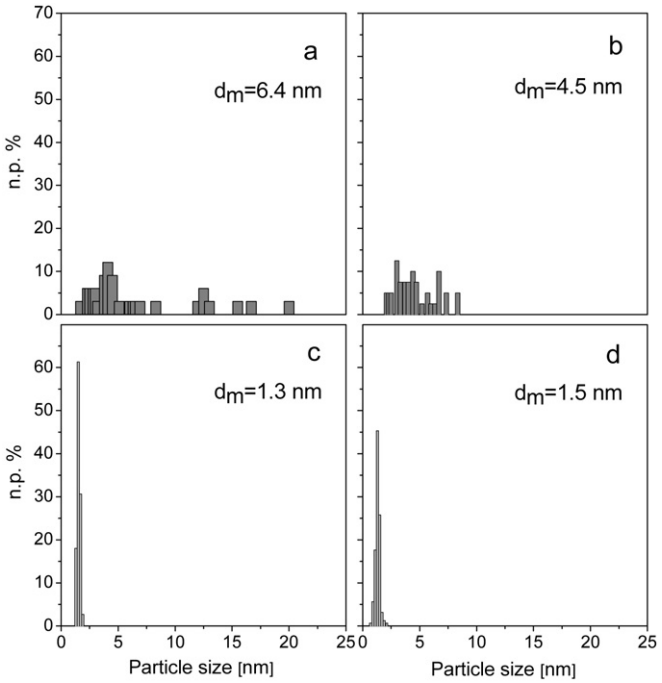

Fig. 3. Pd particles size distributions of ZS–Pd (a), ZS–PdAu (b), CeS–Pd (c), and CeS–PdAu (d).

distribution related to this sample is broad indicating a large heterogeneity in size with a significant fraction larger than 10 nm. The average diameter of the particles observed on ZS–PdAu is 4.5 nm (Fig. 3b) and the relative size distribution is broad but particles never exceed 10 nm. The presence of gold seems to have an ef-

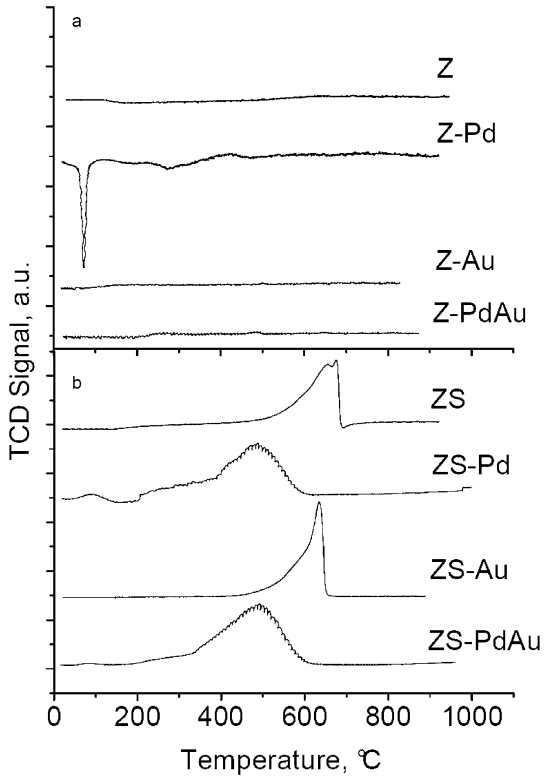

Fig. 4. TPR profiles of fresh calcined catalysts supported on zirconia (a) and sulfated zirconia (b).

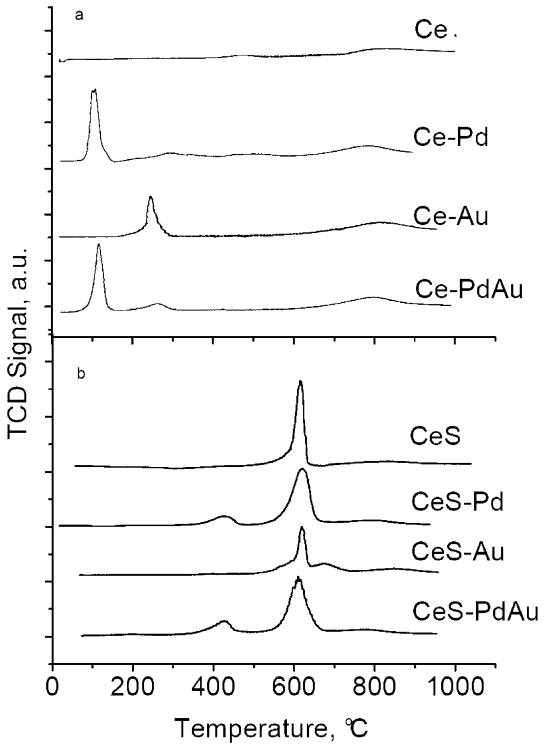

Fig. 5. TPR profiles of fresh calcined catalysts supported on ceria (a) and sulfated ceria (b).

fect on the final dimensions of metallic particles, decreasing their size.

Finally, we found very similar particle size in both CeS supported catalysts (Figs. 3c and 3d), where the average diameter is 1.3 nm for CeS–Pd and 1.5 nm in the case of CeS–PdAu. Differently from the samples supported on zirconia, no separate large gold particles have been detected in this case. Additionally, the particle size distributions are very narrow and no effect of the presence of gold on the morphology and dimensions is evidenced.

3.3. TPR analysis of fresh catalysts

After metal deposition and calcination, a TPR analysis was performed to investigate the metal oxidation state and in the case of bimetallic samples to identify possible interactions between palladium and gold.

Fig. 4 shows the TPR analyses for zirconia (a) and sulfated zirconia (b) samples. The TPR profiles of ZrO_2 support and of Au/ZrO_2 catalyst are completely flat and they do not show any feature. This means that all gold sites on this support are already metallic at room temperature after calcination. Instead, the TPR profile of palladium on zirconia catalyst shows a negative peak at about 70 °C, which corresponds to hydrogen evolution, as identified by mass spectroscopy. It must be remembered that the TPR testing set up requires the reducing mixture pass through the samples to be analyzed to clean the apparatus, prior to starting the temperature ramp. This procedure can cause PdO reduction already at room temperature. If the Pd metal particles are large enough, they can lead to the formation of Pd β-hydride [40,41], which decomposes at about 70 °C. In agreement with the above, the negative peak at about 70 °C in the Z–Pd TPR profile can be assigned to Pd β-hydride decomposition. As there are no other peaks, this means that monometallic palladium sample on zirconia contains only room temperature reducible Pd(II) species. On the contrary the TPR profile of bimetallic palladium–gold catalyst is completely flat and does not show the negative peak of the Pd β-hydride decomposition. It has been noted [42,43] that disappearance, or strong decrease of the Pd hydride decomposition peak in TPR experiments may be a good evidence of Pd alloying, when Pd dispersion is not high. However, our spectroscopic characterization does not allow to evidence alloy formation.

The TPR profile of sulfated zirconia support, reported in Fig. 4b, shows a peak at about 650 °C that is due to sulfate reduction mainly to SO_2 and in part to H_2S [33], as indicated by parallel MS analysis. This peak becomes broad and shifted to lower temperature (around 500 °C) in ZS–Pd and ZS–PdAu catalysts. Mass spectroscopy shows that it is almost completely due to H_2S evolution, meaning that the presence of Pd catalyzes sulfate reduction. On the contrary the TPR profile of gold-based catalyst is similar both in shape and position to that of the support, showing that gold does not influence the SO_4^{2-} reduction. In these sulfated zirconia samples in addition to sulfate reduction, the presence of broad and small peaks at about 100 °C only in the palladium containing catalysts should be noticed, meaning that in these samples the metal is not completely reducible at room temperature. Instead, the ZS–Au TPR profile shows only the peak related to sulfate reduction, indicating that in this sample the metal is completely reduced already at ambient temperature.

Fig. 5 shows the TPR analyses for ceria (a) and sulfated ceria (b) samples. The TPR spectrum of pure ceria shows two reduction peaks, one located at about 500 °C and the other one at 820 °C. The first one can be related [44] to the reduction of surface oxygen species, while the high temperature-peak is related to the reduction of bulk oxygen and the formation of defective cerium oxide. As previously reported [44], the latter peak, is not influenced by gold addition (Ce–Au sample). On the contrary, in the presence of palladium, both in Ce–Pd and Ce–PdAu samples, this reduction peak is slightly shifted toward lower temperatures (<800 °C), indicating an easier reduction. The presence of both gold and palladium changes the position of the low-temperature peak. In fact,

in the TPR spectra of Ce–Pd this broad peak shifts from 500 to 300 °C suggesting the possible easier reduction of surface ceria promoted by Pd. Mono- and bimetallic samples supported on non-doped ceria do not show formation of Pd β-hydride, but only a positive peak at about 100 °C, related to the presence of PdO as confirmed by mass spectroscopy, indicating a lower reducibility of Pd when deposited on ceria. The TPR profile of sulfated ceria support, reported in Fig. 5b, shows a peak at about 600 °C due to sulfate reduction mainly to SO_2 and in part to H_2S [33] (MS evidence). In palladium containing catalysts CeS–Pd and CeS–PdAu this peak becomes broad and split in two peaks: one located at about 400 °C, the other at 600 °C, both related to H_2S evolution. The TPR profiles of CeS and CeS–Au are similar, meaning that gold does not influence SO_4^{2-} reduction. Interestingly for all samples supported on sulfated ceria there are no peaks related to metal reduction, meaning that in these cases both gold and palladium are completely reducible already at room temperature. This is a major difference with respect to samples supported on non-doped ceria. No assumptions about Pd–Au alloying can be made, but the absence of the Pd β-hydride peak suggests that Pd is well dispersed in these catalysts [40], in agreement with TEM results.

3.4. Metal dispersion and nature of the exposed sites determined by CO FTIR absorption spectra analysis

An FTIR characterization by CO adsorption has been undertaken on some selected samples differently pretreated in order to get a deeper understanding of the catalyst surface. In the literature some very interesting contributions on the use of IR spectroscopy of adsorbed CO have appeared in the characterization of industrial PdAu catalysts in comparison with model surfaces [45,46], in which the role of the Au promoter has been elucidated. Here, FTIR spectra of CO adsorbed at room temperature on Pd and PdAu catalysts dispersed on both sulfated zirconia and ceria supports have been investigated, in order to gain insight on the metal dispersion and on the nature of the exposed sites after different chemical pretreatments. Experiments in the same conditions have also been performed on monometallic gold samples. At variance with previously examined samples prepared by the deposition–precipitation method [47–49] no bands in the 2100 cm^{-1} region were detected on both ZS-Au and CeS-Au samples. These findings, in agreement with HRTEM results, indicate that the incipient wetness preparation method here adopted produces only large gold particles, unable to adsorb CO.

The spectra of the ZS–Pd and ZS–PdAu samples after CO adsorption at room temperature on the untreated samples (bold curves), on the samples pretreated at room temperature with hydrogen (fine curves) and pretreated with hydrogen and oxygen (dashed curves) are reported in Figs. 6a and 6b. Different bands have been detected in the range of linear (2200–2000 cm^{-1}) and bridged (2000–1700 cm^{-1}) CO carbonyls [50]. Points to be stressed are: (i) the main features of ZS–Pd and ZS–PdAu catalysts are qualitatively very similar, all absorption bands, even changing either the CO pressure or the temperature (not shown for sake of brevity) appear mainly due to CO interacting with palladium sites; (ii) no bands clearly related to gold metallic sites, usually at about 2100 cm^{-1} and completely reversible on outgassing, are evident in the spectra reported in section b; (iii) the FTIR bands of CO on the ZS–PdAu sample are significantly stronger than in the monometallic catalyst both in the case of the untreated samples (bold curves) and in the samples pre-treated both with hydrogen only (fine curves) and with hydrogen and oxygen (dashed curves). Therefore, these data evidence a higher Pd dispersion in bimetallic catalysts, as already evidenced by HRTEM.

A high metal dispersion can produce not only changes in the number of adsorption sites, related to the differences in catalytic

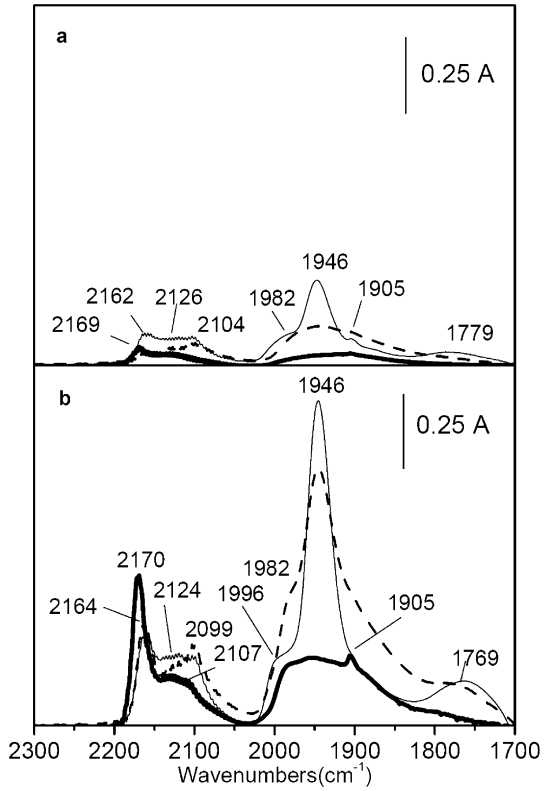

Fig. 6. FTIR spectra of ZS–Pd (a) and ZS–PdAu (b) after CO adsorption at r.t on the as received samples (bold curves), on the samples pretreated at r.t. with hydrogen (fine curves) and pretreated with hydrogen and oxygen (dashed curves). The spectra have been normalized to the same Pd content.

activity, but also in the nature of oxygen adsorption, dissociative or molecular, that can strongly affect the selectivity. In fact, very recently [51], it has been shown by first-principle calculations, that O_2 cannot adsorb dissociatively on very small clusters, as a consequence of the repulsive effects between the two negatively charged atoms. Moreover, changes in morphology and in the exposed facets as a consequence of the composition of the gas phase can be inferred from the spectra of adsorbed CO. The pre-treatment with hydrogen causes an increase of a band at 1946 cm^{-1} on both mono- and bimetallic samples (fine curves). This band is typical of bridge-bonded CO on terrace sites of (111) facets [52] and is almost completely depleted after H_2–O_2 interaction on the ZS–Pd sample (section a, dashed curve), while on the ZS–PdAu catalyst it exhibits only a small decrease in the intensity (section b, dashed curve). This feature can be taken as an indication that terrace sites are mostly retained in the latter catalyst after oxidation yielding a less defective, less energetic surface. In addition, the low frequency component at 1770 cm^{-1} is more intense in the case of the ZS–PdAu sample, possibly as a consequence of a larger back-donation from the metal to the CO molecules, due to an electronic effect of gold under palladium. In summary, although small Au clusters are never directly evidenced by both HRTEM and FTIR, their presence in close proximity of Pd can be inferred by FTIR from the changes in morphology and electron density induced on Pd particles.

A comparison between the catalysts supported on ZS (bold curves) and those supported on CeS (fine curves) is shown in Fig. 7. We reported the spectra, normalized to the same Pd content, related to CO adsorption at r.t. on Pd (a) and Pd–Au (b) untreated samples simply outgassed at r.t.

Differently from the ZS–Pd catalyst (Fig. 7a, bold curve), the CeS–Pd catalyst (Fig. 7a, fine curve) shows a series of well defined and quite strong bands in the carbonyl region after being simply contacted with CO. In particular, components at 2160, 2118,

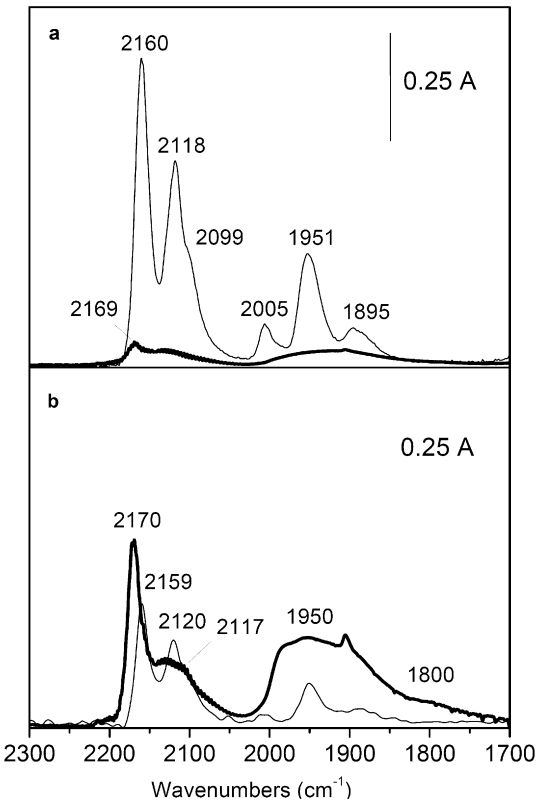

Fig. 7. FTIR spectra of CO adsorbed at r.t. on Pd (a) and Pd–Au (b) untreated samples supported on ZS (bold curves) and on CeS (fine curves). The spectra have been normalized to the same Pd content.

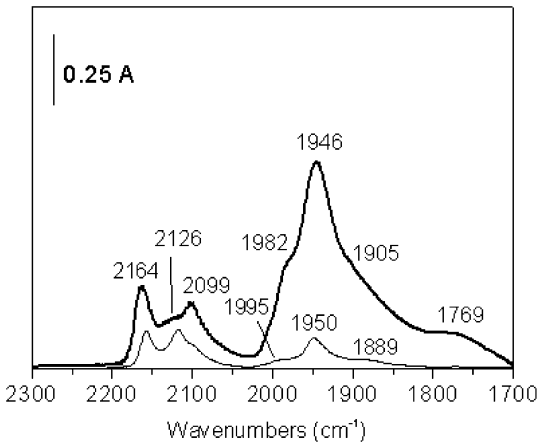

Fig. 8. FTIR spectra of CO adsorbed at r.t. on the ZS–PdAu (bold curve) and CeS–PdAu (fine curve) samples previously contacted with a H_2–O_2 mixture at room temperature. The spectra have been normalized to the same Pd content.

2099, 2005, 1950, and 1895 cm^{-1} are evident, whose overall integrated intensity is noticeably higher than that observed for the CO absorption bands on the ZS–Pd catalyst. These features appear as a strong indication that a larger amount of palladium sites are present at the surface of CeS–Pd in comparison with ZS–Pd. A detailed analysis and assignment of all these features is not within the scope of this work and it will be discussed in a different paper. However, the intensities of the bands related to linearly adsorbed CO on Pd sites (2118–2099 cm^{-1}) are larger than those of bridge bonded CO (2005–1895 cm^{-1}). A high intensity ratio between the linear vs. bridged carbonyls is usually taken as an indication of a small size of the Pd aggregates [53]. The smaller size of the Pd particles detected by HRTEM on CeS–Pd with respect to ZS–Pd is in agreement with the FTIR findings.

The band patterns detected in the carbonyl region on both bimetallic catalysts (Fig. 7b) are the same as those detected on the monometallic samples (Fig. 7a). However, the intensity is completely opposite if compared to that observed for the Pd catalysts, since the bands related to ZS–PdAu (bold curve) are now more intense than those observed for CeS–PdAu (fine curve) after the interaction with CO at r.t. Moreover, the intensity of the carbonyl bands of ZS–PdAu is also higher than that related to the absorptions observed on ZS–Pd, indicating the presence of a larger fraction of exposed sites, hence a higher metal dispersion, in agreement with HRTEM observations.

Gold adsorbs at room temperatures only on highly uncoordinated step sites of small particles at relatively high equilibrium pressures, therefore it can be suggested that the round shaped particles of about 100 nm observed in some regions of HRTEM micrographs of ZS–PdAu are likely made of pure gold and do not adsorbs CO in our experimental conditions. The differences observed between ZS–PdAu and ZS–Pd, only relative to the intensity of the bands, without any effect on the frequency and on the relative intensity between the on-top and the bridged CO FTIR absorption band, strongly indicate that an alloying between Pd and Au is very unlikely at the surface of the metallic particles. Anyhow, an effect of gold addition on Pd dispersion is evident and could possibly be related to the growth of a palladium layer on top of gold small particles as suggested by Herzing et al. on Au–Pd/Al_2O_3 catalysts, subjected to a variety of heat treatments [54].

As for the CeS-supported catalysts, the bands related to the monometallic sample are qualitatively the same as those related to the bimetallic one, but they are more intense in the former case. This feature cannot be related, analogously to the ZS-supported catalysts, to the different size of the metallic particles exposed at the surface of the two samples, because the HRTEM analysis found very similar average diameters. Hence, being the FTIR spectra normalised to the same palladium content, being the average particle sizes on the two catalysts practically the same as well as the pretreatment to which the samples have undergone, the difference in band intensity can be ascribed to an effect related to the presence of gold.

3.5. Effect of the H_2–O_2 pretreatment on the surface oxidation state of the bimetallic samples determined by CO FTIR absorption spectra analysis

We also studied the CO interaction with the bimetallic samples previously contacted at room temperature with a H_2–O_2 mixture (Fig. 8) as these pre-treatment conditions strongly influence the catalysts activity and selectivity (see Section 3.7). The absorption bands of CO adsorbed on CeS–PdAu (fine curve) are all quite weak, similarly to what observed on the same untreated sample simply outgassed at r.t.. Moreover, the intensity ratio of the on top carbonylic species and the bridged ones on the CeS–PdAu both in pure CO and in CO adsorbed after H_2–O_2 interaction are quite similar, only a small reduction of the amount of the exposed sites is observed and no changes in their nature and relative abundance is evidenced. On the contrary, the bands produced by the same interaction on the ZS–PdAu sample (bold curve) appear much stronger. Also different is the bridged/linear intensity ratio that is much higher in the ZS–PdAu sample compared to the CeS-PdAu sample. The differences can possibly be understood considering the different nature of the two supports. Ceria can be quite easily reduced close to the metallic particles already under mild conditions producing oxygen vacancies with oxygen migrating on the small metallic particles [55]. Additionally, a large fraction of the palladium sites of the CeS–PdAu sample, may be present as PdO after treatment with H_2–O_2. These sites are no longer detectable

Table 3
Kinetic constants of ZS–Pd and CeS–Pd monometallic samples using different gas mixtures

Sample	Gas feed	$k'_1 \times 10^4$ ($mol\,L^{-1}\,min^{-1}$)	$k'_2 \times 10^4$ ($mol\,L^{-1}\,min^{-1}$)	$k'_3 \times 10^3$ (min^{-1})
ZS–Pd	10/10	5.0	11.3	14.5
ZS–Pd	4/10	2.4	11.1	5.0
ZS–Pd	4/96	2.8	8.1	1.4
CeS–Pd	10/10	5.5	3.8	7.5
CeS–Pd	4/10	1.3	1.7	1.7
CeS–Pd	4/96	0.6	2.8	0.00003

by CO adsorption. It has been shown that the oxidation mechanism of Pd is strongly dependent on the particle size [56], in the size range <3 nm the stoichiometry corresponds to PdO. In a study of a model Pd/Fe_3O_4 sample by multimolecular beam experiments [53], it has been found that the formation of Pd oxide species occurs preferentially at the particle/support interface, while the region of particles more remote from the support, i.e., on top of the Pd interface oxide, remains metallic when the particles are larger than 3 nm. The nature of the support play a prominent role on the formation and stabilization of oxidized particles. The oxidation process appears easier on ceria than on zirconia, possibly as a consequence of the oxygen storage-release properties and also of the smaller size of the metallic particles detected on both the CeS-supported catalysts, in agreement with HRTEM observations.

3.6. Reactivity with monometallic catalysts without pretreatment

The major problem of this process is the low selectivity because of the complex reaction network involving hydrogen and oxygen (Scheme 1). First of all, preliminary tests of H_2O_2 decomposition were carried out on pure calcined ceria and sulfated ceria under the conditions used in the catalytic tests (20 °C, 1 bar, 5 h) in order to verify that they did not decompose H_2O_2. Similar tests on zirconia supports were already positively investigated [26].

Most oxidation reactions involving H_2O_2 are carried out in organic solvents, often in methanol. The direct synthesis of this chemical in this solvent could be an advantage from a practical point of view avoiding separation and concentration costs [25].

Results of catalytic tests with different gas feeds on sulfated zirconia are shown in Figs. 9a and 9b and Table 3. Experiments carried out by feeding an undiluted hydrogen/oxygen mixture, where oxygen was in large excess (4/96), display a completely different behavior with respect to tests with the two ternary H_2/air/N_2 gas mixture. In the former case the productivity is comparably lower at the beginning, but shows very good values on long reaction times because it remains stable reaching about 400 $mmol_{H_2O_2}/g_{Pd}\,h$ after 5 h, when concentrations up to 67 mM H_2O_2 were observed corresponding to to about 0.3 wt% were observed. On the contrary, with both diluted hydrogen/air/nitrogen mixtures no increase in productivity is observed after about 2 h. This means that, beyond this point, H_2O_2 decomposition starts prevailing over H_2O_2 formation.

The positive result obtained using the undiluted hydrogen/oxygen mixture is to be ascribed to the excess of oxygen and not to the low hydrogen content (see results obtained with the 4/10 gas feed). Moreover, it is very interesting to note that while catalyst selectivity decreases with time in tests with diluted feeds, it is higher and stable (around 20%) for several hours under undiluted test conditions (4/96). As a consequence under these conditions water production is low.

Fitting the catalytic curves of sulfated zirconia samples according to the procedure specified in Section 2, yielded the parameters reported in Table 3. The test under the 10/10 gas feeding has a comparably high k'_1 (almost double with respect to the others), but also the highest k'_2 and k'_3. This means that over the first hour the high hydrogen concentration, promotes Pd reduction increasing the activity, but then this excess of hydrogen favors water formation.

Test under the 4/10 feeding has about the same k'_2 value of the one under the 10/10 feeding, showing that water direct synthesis is hardly influenced by hydrogen concentration. Instead, the test in hydrogen/oxygen undiluted mixture presents the lowest k'_2 value and, most interestingly, the lowest k'_3 value, which is almost 10 times lower than that calculated in the 10/10 gas feeding. This slow water formation by direct synthesis and by hydrogen peroxide reduction leads to a higher and stable H_2O_2 selectivity under undiluted test conditions (4/96), mainly because of the excess of oxygen rather than hydrogen concentration.

Catalytic tests over non-doped zirconia sample give lower catalytic activity and lower selectivity than sulfated zirconia catalyst. For example, using undiluted test conditions (4/96), Z–Pd catalyst reaches about 100 $mmol_{H_2O_2}/g_{Pd}\,h$ (<15% selectivity) after 5 h time on stream, while ZS–Pd about 400 $mmol_{H_2O_2}/g_{Pd}\,h$ (<20% selectivity).

Results of catalytic tests with different gas feed on sulfated ceria, shown in Figs. 9c and 9d, allow the following observations: (i) in the case of CeS–Pd the 10/10 gas feeding is the best one, reaching about 500 $mmol_{H_2O_2}/g_{Pd}\,h$ after 3 h of time on stream. Within 5 h, concentrations of 66 mM H_2O_2 were produced; (ii) under the same test conditions CeS–Pd shows a significant improvement in catalytic performance with respect to ZS–Pd sample, which gives concentrations of 35 mM H_2O_2 after 5 h of time on stream; (iii) selectivity drops down to low values under both diluted gas feeds, similarly to sulfated zirconia samples; (iv) the 4/96 feed is the only one that, even if productivity is low (it reaches only 20% of the productivity of the 10/10 gas feed), allows to obtain a moderately increasing selectivity (<18%). Table 3 summarizes the parameters calculated by fitting the catalytic curves for CeS–Pd sample, and they confirm the previous observations. It can be noted that the 10/10 feed yields the highest k'_1 value, but also the highest constants for water formation (k'_2 and k'_3). Catalytic test with the 4/96 gas mixture yields very low k'_1, k'_2, and k'_3, but k'_3 is 10^{-5} times lower than the k'_3 of the 10/10 and 4/10. Ceria support is characterized by high oxygen storage capacity (OSC) and reducibility and probably this allows to improve the catalytic activity even in reactions with a relatively high hydrogen concentration in the gas feed.

Catalytic tests were performed with the three gas mixtures also for the Ce–Pd sample, but the achieved productivity is only half of the corresponding test with CeS-Pd sample. For example after 3 h time on stream with the undiluted hydrogen/oxygen feed, productivity is 69 $mmol_{H_2O_2}/g_{Pd}\,h$ for the Ce–Pd sample (<14% selectivity), vs 112 $mmol_{H_2O_2}/g_{Pd}\,h$ for the CeS–Pd catalyst (<20% selectivity); with the 10/10 gas mixture the difference is 245 vs 500 $mmol_{H_2O_2}/g_{Pd}\,h$. Also for ceria based catalysts sulfation allows higher catalytic activity and selectivity.

TPR analysis of the used samples shown in Fig. 10, can help to understand the differences in catalytic results reported above. First of all, it is evident (Fig. 10b) that Pd in CeS-Pd sample is completely reduced during catalytic tests. This is shown by the presence of the Pd β-hydride decomposition peak, and the absence of any reduction peak in the same region. On the contrary, in all used non-sulfated ceria supported samples (Fig. 10a) there is a hydrogen consumption at about 100 °C related to metal reduction. This means that palladium is not completely reduced during catalytic tests in nondoped ceria supported catalysts. It is possible that the lower productivity values obtained with Ce–Pd sample with respect the CeS–Pd sample can be ascribed to this incomplete reducibility, due to a strong interaction of palladium with ceria support.

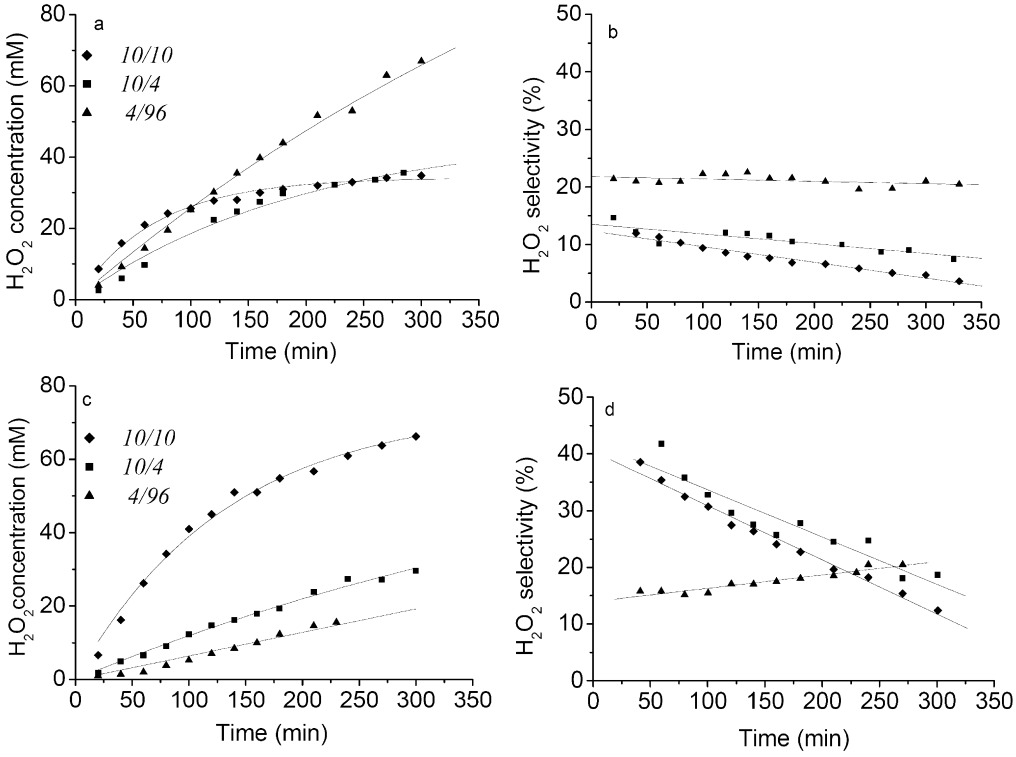

Fig. 9. Catalytic activity (a) and selectivity (b) toward H_2O_2 for ZS–Pd sample and activity (c) and selectivity (d) toward H_2O_2 for CeS–Pd sample during kinetics tests under different gas feed (◆) 10/10; (■) 10/4; (▲) 4/96.

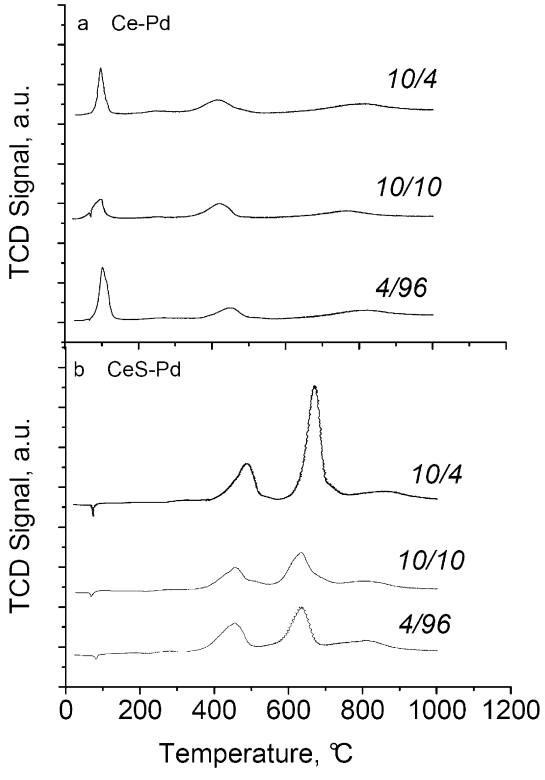

Fig. 10. TPR profiles of monometallic palladium-based used catalysts supported on ceria (a) and sulfated ceria (b) after kinetic tests under different gas feed.

3.7. Reactivity with monometallic catalysts after a reductive–oxidative pretreatment

Recently we have investigated the effect of the Pd oxidation state in H_2O_2 direct synthesis, and have shown [26] that surface oxidized Pd^0 catalysts have a high catalytic activity and the highest selectivity. The apparent discrepancy with the results reported above for the incompletely reduced Ce–Pd sample requires a distinction between incomplete reduction and surface oxidation. Catalysts must be fully reduced to display their maximum activity and selectivity, but a surface Pd oxidation allows to increase both. To check this point particle surface oxidation was tested also with these catalysts. To this purpose, catalysts were reduced in situ by passing a pure hydrogen flow into the reaction medium (after the usual de-aeration step). This led to a completely reduced catalyst. Then, pure oxygen was fed. Excess oxygen was subsequently removed by passing pure nitrogen. The three different mixtures (10/10, 4/10, 4/96) were finally fed into the reactor. The results are shown in Fig. 11 and Table 4. For the ZS–Pd sample (Figs. 11a and 11b), surface oxidation induced a higher catalytic activity for all three different feedings. In particular, productivity after 3 h time on stream for the 10/10 is three times higher than with the non-pretreated sample (870 vs 288 $mmol_{H_2O_2}/g_{Pd}$ h, respectively), it is two times higher (550 vs 277 $mmol_{H_2O_2}/g_{Pd}$ h) for the 4/10 feed and increases significantly (670 vs 410 $mmol_{H_2O_2}/g_{Pd}$ h) for the 4/96 feed. Maximum H_2O_2 produced was 90 mM, which corresponds to 0.38 wt%. The reaction profiles in terms of activity and selectivity after a reductive/oxidative pretreatment (Figs. 11a and 11b) are the same as without any pretreatments (Figs. 9a and 9b). Again, the undiluted hydrogen/oxygen mixture allows to obtain a linear H_2O_2 production and a constant selectivity, higher than that of the reaction without any pretreatments (50 vs 23%). Selectivity of the reactions under 10/10 and 4/10 gas mixtures are higher with respect to the fresh samples. An inspection of pseudo-kinetic constants collected in Table 4 allows the following observations for the ZS–Pd sample after the reduction/oxidation pretreatment: (i) k_1' are higher for the three different feeds, and this can explain the significant improvement in catalytic performance with respect to the fresh sample; (ii) k_2' are lower for the three different feeds, explaining the increase in selectivity with re-

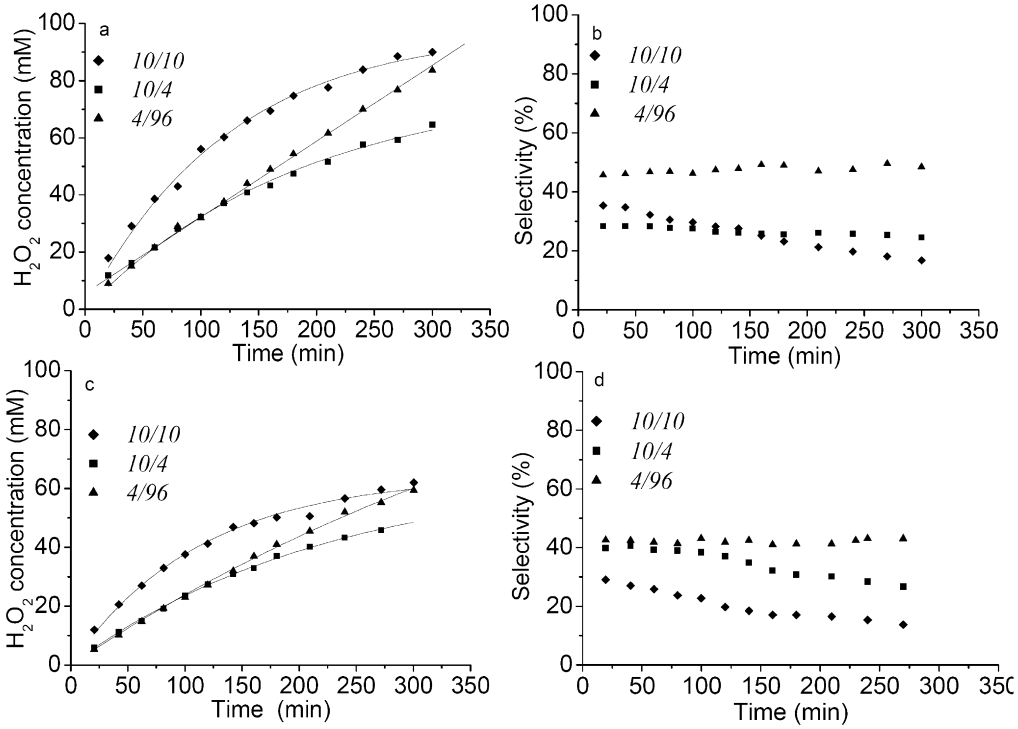

Fig. 11. Catalytic activity and selectivity toward H_2O_2 during kinetics tests under different feeding for ZS–Pd (a and b), CeS–Pd (c and d) after a reductive–oxidative pretreatment.

Table 4
Kinetic constants for samples tested under different gas feed after the reductive–oxidative pretreatment

Sample	Gas feed	$k'_1 \times 10^4$ (mol L^{-1} min^{-1})	$k'_2 \times 10^4$ (mol L^{-1} min^{-1})	$k'_3 \times 10^3$ (min^{-1})
ZS–Pd	10/10	7.9	5.8	8.0
ZS–Pd	4/10	4.2	0.4	5.3
ZS–Pd	4/96	3.6	1.9	1.8
ZS–PdAu	4/96	4.6	0.3	2.8
Z–PdAu	4/96	4.0	0.1	2.9
CeS–Pd	10/10	5.7	7.6	8.8
CeS–Pd	4/10	2.9	3.3	4.4
CeS–Pd	4/96	2.6	2.0	1.9
CeS–PdAu	4/96	2.2	1.6	2.6
Ce–Pd	10/10	5.3	3.2	7.8
Ce–Pd	4/10	3.4	1.6	5.0
Ce–Pd	4/96	2.8	1.9	0.9
Ce–PdAu	4/96	2.5	1.1	4.1

spect to the fresh sample; (iii) k'_3 in hydrogen/oxygen mixture is lower than the values of the reactions in air diluted feeds.

Results of catalytic tests with different gas feeds on sulfated ceria after a reduction/oxidation pretreatment are shown in Figs. 11c and 11d and kinetic data are reported in Table 4. As can be seen in the case of CeS–Pd, the 10/10 gas feed is the best one, but there is no improvement in productivity with respect to the fresh catalyst under the same reaction conditions (productivity < 500 $mmol_{H_2O_2}/g_{Pd}$ h after 3 h for the fresh catalyst, 458 after pretreatment). This is confirmed by the k'_1 values, which are similar (respectively 5.7 and 5.5×10^{-4} mol/L min). On the contrary the two gas mixtures with only 4% hydrogen increase productivity and selectivity after the reduction/oxidation pretreatment. Tables 3 and 4 show that in these cases (4/10 and 4/86) the k'_1 values are higher after the reduction/oxidation pretreatment. Moreover, in the reaction under the 4/96 gas feeding, productivity after 5 h for the red-ox treated CeS–Pd sample reaches a value similar to the best one of the same sample, obtained with the air diluted 10/10 gas mixture. Nevertheless, in the reaction with the undiluted mixture the selectivity is constant (<40%) after pretreatment. The parameters calculated by fitting the catalytic curves for CeS–Pd sample after red-ox pretreatment confirm the previous observations. The 4/96 gas feeding shows a lower k'_1 value than the 10/10 gas feeding, but also much lower constants for water formation (k'_2 and k'_3).

A comparison of the catalytic results obtained after the red-ox pretreatment on sulfated zirconia and sulfated ceria samples demonstrated that both productivity and selectivity are higher in the case of ZS–Pd catalyst for the three different gas feeds.

Also the red-ox pretreated Ce–Pd sample achieved much higher productivity than the corresponding fresh sample. The most important result is the productivity under the undiluted hydrogen–oxygen gas feeding, that is six times higher than without any pretreatments (respectively 420 vs 69 $mmol_{H_2O_2}/g_{Pd}$ h after 3 h and 395 vs 71 $mmol_{H_2O_2}/g_{Pd}$ h after 5 h). For the same reaction conditions selectivity increases from 14 to 55% after the red-ox pretreatment and it is constant over the 5 h test.

From TPR analysis of the used sample (not shown for the sake of simplicity) it is evident that Pd in pretreated Ce–Pd sample is completely reduced after catalytic tests. On the contrary, Pd in non-pretreated Ce–Pd sample is not completely reducible during catalytic tests, as previously reported. Notably, after red-ox pretreatment, the non-doped ceria supported catalyst shows higher catalytic activity and selectivity than the sulfated ceria sample for the three gas feeds.

Also Au catalysts supported on zirconia and ceria both sulfated and non-sulfated were tested in the direct hydrogen peroxide synthesis under different gas feeds. No H_2O_2 or H_2O production was ever observed under our experimental conditions. On the other hand, other Au catalysts reported in the literature, either more dispersed and/or tested under more severe conditions [17,57], were found far less active than Pd containing catalysts.

3.8. Reactivity of bimetallic catalysts

The effects of the addition of gold, in order to improve H_2O_2 productivity and selectivity was investigated. Some authors have

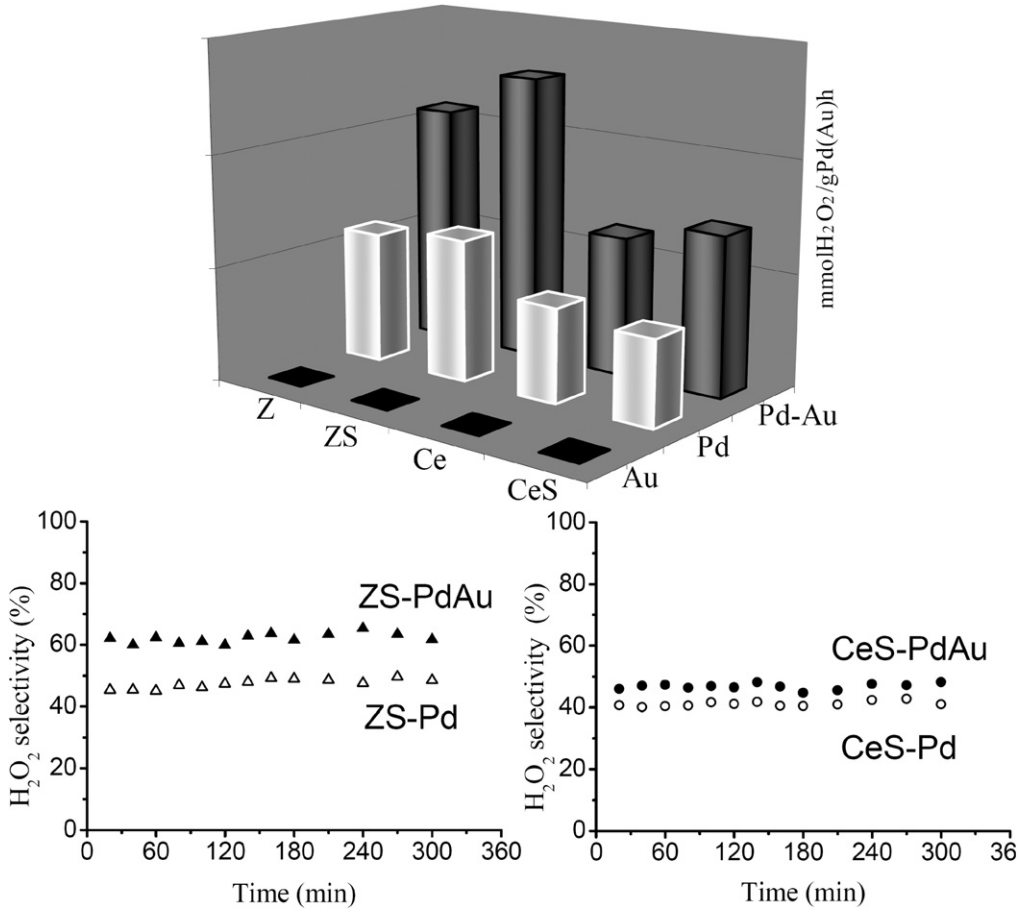

Fig. 12. Productivity (at 3 h of reaction under 4/96 after a reductive–oxidative pretreatment) and selectivity for mono- and bimetallic samples.

shown, working either under pressure [14,17,18], or under explosive conditions [58] that bimetallic catalysts based on Au–Pd can provide a significant improvement in hydrogen peroxide formation compared to Pd only catalysts. In Fig. 12 a comparison between mono- and bimetallic samples during a catalytic test under the 4/96 gas feeding and after the red-ox pretreatment is reported. A comparison of the results of the bimetallic ZS–PdAu sample with respect the corresponding monometallic Pd catalyst, shows that gold addition really improves not only the catalytic activity but also H_2O_2 selectivity. In fact H_2O_2 productivity increases from 670 for the ZS–Pd sample to 1270 $mmol_{H_2O_2}/g_{Pd}$ h for the ZS–PdAu catalyst after 3 h of reaction. The most important result is however the improvement in selectivity (50 vs 61%), still constant for several hours (Fig. 12). The latter value is indeed very high considering that it is obtained with a low Pd containing catalyst and is stable even after 5 h of reaction. Besides, it should be noted that also for bimetallic catalysts the use of a sulfated support induced a higher catalytic activity with respect the non-doped sample: productivity increases from 1070 to 1270 $mol_{H_2O_2}/g_{Pd}$ h after 3 h time on stream, and selectivity shows also a remarkable improvement (from a constant value of 40–61%). In Table 4 the kinetic constants for ZS–PdAu and Z–PdAu samples are collected. It is interesting to note that: (i) in both bimetallic catalysts k_1' is higher than in the monometallic ZS–Pd sample, and this can explain the improvement in catalytic performance; (ii) k_2', the constant associated with direct water formation, decreases remarkably for both bimetallic catalysts, explaining the increase in selectivity with respect to the monometallic sample.

In order to test the stability and reusability of the bimetallic samples, we carried out some catalytic tests with a used ZS–PdAu catalyst, after filtration and drying. Both productivity and selectivity remained unchanged after three cycles, showing the good reusability of our samples. Moreover, after catalyst filtration the resulting solution did not show any residual activity, confirming that there is no metal leaching from the catalyst.

In Fig. 12, H_2O_2 production and selectivity for the two bimetallic samples supported on ceria and sulfated ceria are reported. Both productivity and selectivity are similar for CeS–PdAu and Ce–PdAu samples during catalytic tests under the 4/96 gas feed and after the red-ox pretreatment. A comparison with the results of the monometallic samples shows an improvement in H_2O_2 productivity for both bimetallic catalysts (after 3 h: 720 $mol_{H_2O_2}/g_{Pd}$ h for CeS–PdAu and 370 $mol_{H_2O_2}/g_{Pd}$ h for CeS–Pd; 620 $mol_{H_2O_2}/g_{Pd}$ h for Ce–PdAu and 420 $mol_{H_2O_2}/g_{Pd}$ h for Ce–Pd). Additionally selectivity is slightly increased for the sulfated ceria supported sample.

TPR analyses of the used bimetallic samples are shown in Fig. 13, and can help to understand some of the catalytic results reported above. First of all, both palladium and gold in all samples are completely reduced during catalytic tests. This is shown by the presence of the Pd β-hydride decomposition peak, albeit small, and the absence of any reduction peak in the same region. Interestingly, all samples show reduction peaks that can be associated to sulfate decomposition. As already observed for zirconia supported catalysts [26], sulfate ions, coming from sulfuric acid added to acidify the solution in catalytic tests, can adsorb on the un-promoted support surface changing it into an actually sulfated sample. For CeS–PdAu and Ce–PdAu the peaks associated with sulfate reduction are very similar, and this can explain the similar behavior of these samples.

In summary, the addition of Au to the the monometallic Pd samples causes an increase in activity as well as selectivity with both zirconia and ceria support. While the increase in activity can

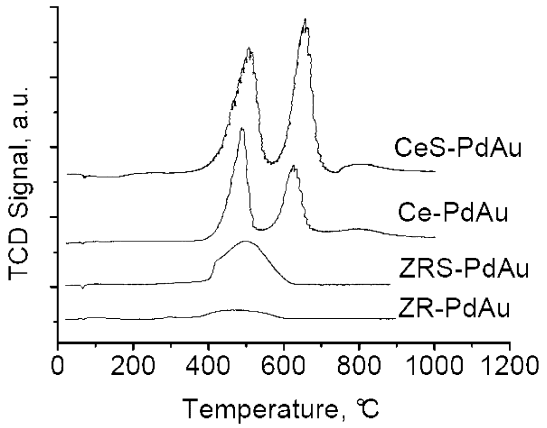

Fig. 13. TPR profiles of used bimetallic catalysts after kinetic tests under 4/96 gas feeding after a reductive–oxidative pretreatment.

be easily traced back to the presence of smaller metal particles in bimetallic samples, as evidenced by HRTEM, the increase in selectivity requires a different explanation.

3.9. Possible reaction pathway

Recently, we proposed a possible reaction pathway for the formation of hydrogen peroxide on monometallic Pd catalysts [24]. As reported in Fig. 14, according to this proposal oxygen can chemisorb with or without dissociation depending on the chemisorption sites that can be more or less energetic. Chemisorption on non-defective (less energetic) Pd sites occurs without dissociation, a necessary condition to give the desired H_2O_2 product. Then, protonation from external H^+ takes place, a quite well-known process in side-on Pd peroxo complexes [59] followed by reaction with H_2 leading to the formation of H_2O_2 and restoring H^+. At the same time more energetic sites (defects, edges, corners, etc.) will dissociatively chemisorb O_2 or readsorb H_2O_2. The presence of chemisorbed hydrogen will lead to the formation of water either directly by reaction with oxygen atoms or by reaction with OH fragments coming from H_2O_2. This view is consistent with the increase in hydrogen peroxide selectivity observed in a large excess of oxygen, i.e. when 4/96 feed conditions are employed. The data reported in this paper for monometallic catalysts are consistent with this interpretation.

Now the question arises whether this possible reaction pathway can hold also for Pd–Au bimetallic catalysts. Reactivity results have demonstrated that the addition of gold, although not directly involved in the reaction, is capable to increase significantly the activity of the bimetallic catalysts as a consequence of a better dispersion of the Pd active component. However, as was shown by IR investigation, this does not correspond to an increase in the number of more energetic active sites, as one would expect. A higher fraction of terrace sites is observed as well as an increase in hydrogen peroxide selectivity. From this point of view the pathway suggested in Fig. 14 seems to hold also for bimetallic samples.

In this respect another important argument has been recently suggested in the literature. Hutchings and co-workers have recently demonstrated that upon calcination at 500 °C a Au-rich core/Pd-rich shell morphology is induced in Pd–Au bimetallic catalysts on different supports [17,18,54,60,61]. This morphology can apply also to the present case given the experimental procedure followed for catalyst preparation. It can be suggested that the Au core would exert an electron donation effect on the Pd shell that would justify the existence of the 1770 cm^{-1} band in the FTIR spectrum. This would make Pd more "noble," less reactive toward oxygen, decreasing dissociative chemisorption on more energetic sites.

Hence, the role of gold in the catalytic reaction seems to be a complex one, improving the performance of Pd particles changing their size, morphology and electron density and making them more suited to the reaction requirements.

4. Conclusions

In this work mono- and bimetallic palladium–gold catalysts supported on zirconia and ceria both sulfated and non-sulfated were successfully tested for the direct synthesis of hydrogen peroxide under very mild conditions (1 bar and 20 °C) and outside the explosion range. Support sulfation was found to be beneficial for productivity especially in bimetallic samples. Although gold by itself is not active in catalysis and gold small particles are not evidenced by HRTEM it must be in close contact to Pd as its presence profoundly changes both Pd dispersion, morphology and electron density as evidenced by HRTEM and FTIR. As already mentioned above, some authors have found segregation of Au in the core of bimetallic particles, giving rise to a Au-rich core/Pd-rich shell morphology. Although the preparation conditions may justify a similar assumption also in the present case, the nature of Pd–Au interaction remains poorly understood and will be the subject of further studies. A critical point would be understanding why a decrease in particle size in Pd–Au samples is associated to a larger portion of terrace sites as suggested by FTIR.

Monometallic Pd samples yield the best catalytic results using the sulfate doped zirconia support, while monometallic gold catalysts show neither hydrogen peroxide nor water production under the mild experimental conditions used. On the contrary, in bimetallic Pd–Au catalysts the addition of Au improves the productivity and in particular the selectivity of the process.

Gas feed composition is crucial to improve catalyst performance. Using H_2/O_2 mixtures containing a large excess of oxygen virtually stops the consecutive H_2O_2 hydrogenation reaction resulting in a steady productivity over time and a constant selectivity.

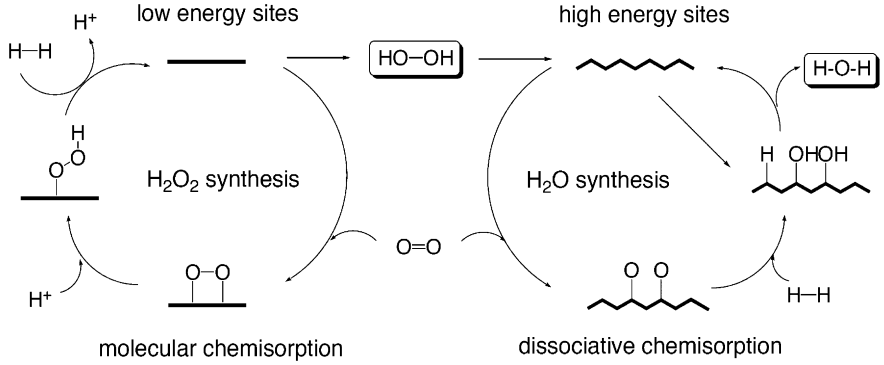

Fig. 14. Possible pathway for the synthesis of H_2O_2 and H_2O on mono- and bimetallic Pd–Au catalysts.

A high oxygen concentration in the feed is a medium to maintain the Pd surface oxidized. This effect is magnified by a reduction–oxidation pretreatment that allows to achieve with the ZS–PdAu catalyst a maximum 100 mM H_2O_2 production corresponding to 0.43 wt%, and a 61% selectivity stable even after 5 h. Catalyst recycling without loss of activity and selectivity is also an important issue in evaluating the performance of these catalysts.

Oxygen adsorption without dissociation is a necessary condition to hydrogen peroxide formation. The surface oxidation effect is consistent with a possible reaction pathway involving oxygen adsorption without dissociation on low energy sites and minimizing hydrogen chemisorption. These features maximize hydrogen peroxide production and minimize water formation. Consistently, the addition of Au decreases Pd particle size increasing productivity while at the same time maintaining a high proportion of low energy sites increasing selectivity.

Acknowledgments

We thank MIUR (Rome) for financial support through PRIN 2006 program.

References

[1] B. Notari, Adv. Catal. 41 (1996) 253.
[2] Chemical Week, August 17, 2005.
[3] Chemical Week, July 2–9, 2003, 44.
[4] H.-J. Riedl, G. Pfleiderer, US patent 2215883, 1940.
[5] L.W. Gosser, US patent 4681751, 1987.
[6] L.W. Gosser, J.T. Schwartz, US patent 4772485, 1988.
[7] J. Van Weynbergh, J.-P. Schoebrechts, US patent 5447706, 1995.
[8] B. Bertsch-Frank, I. Hemme, S. Katusic, J. Rollmann, US patent 6387364, 2002.
[9] G. Paparatto, R. D'Aloisio, G. De Alberti, R. Buzzoni, US patent 6630118, 2003.
[10] K.M. Vanden Bussche, S.F. Abdo, A.R. Oroskar, US patent 6713036, 2004.
[11] T.A. Pospelova, N.I. Kobozev, E.N. Eremin, Russ. J. Phys. Chem. 35 (1961) 143.
[12] R. Burch, P.R. Ellis, Appl. Catal. B 42 (2003) 203.
[13] D.P. Dissanayake, J.H. Lunsford, J. Catal. 214 (2003) 113.
[14] P. Landon, P.J. Collier, A.J. Papworth, C.J. Kiely, G.J. Hutchings, Chem. Commun. (2002) 2058.
[15] V.V. Krishnan, A.G. Dokoutchaev, M.E. Thompson, J. Catal. 196 (2000) 366.
[16] A.G. Gaikwad, S.D. Sansare, V.R. Choudhary, J. Mol. Catal. A 181 (2002) 143.
[17] J.K. Edwards, B. Solsona, P. Landon, A.F. Carley, A. Herzing, M. Watanabe, C. Kiely, G. Hutchings, J. Mater. Chem. 15 (2005) 4595.
[18] J.K. Edwards, B. Solsona, P. Landon, A.F. Carley, A. Herzing, C. Kiely, G. Hutchings, J. Catal. 236 (2005) 69.
[19] T.A. Pospelova, N.I. Kobozev, Russ. J. Phys. Chem. 35 (1961) 262.
[20] K. Otsuka, I. Yamanaka, Electrochim. Acta 35 (1990) 319.
[21] I. Yamanaka, T. Hashimoto, K. Otsuka, Chem. Lett. (2002) 852.
[22] Y. Ando, T. Tanaka, Int. J. Hydrogen Energy 29 (2004) 1349.
[23] J. Zhou, H. Guo, X. Wang, M. Guo, J. Zhao, L. Chen, W. Gong, Chem. Commun. (2005) 1631.
[24] S. Abate, G. Centi, S. Melada, S. Perathoner, F. Pinna, G. Strukul, Catal. Today 104 (2005) 323.
[25] S. Melada, F. Pinna, G. Strukul, S. Perathoner, G. Centi, J. Catal. 237 (2006) 213.
[26] S. Melada, R. Rioda, F. Menegazzo, F. Pinna, G. Strukul, J. Catal. 239 (2006) 422.
[27] V.R. Choudhary, C. Samanta, J. Catal. 238 (2006) 28.
[28] J.K. Edwards, A. Thomas, B. Solsona, P. Landon, A.F. Carley, G. Hutchings, Catal. Today 122 (2007) 397.
[29] X. Song, A. Sayari, Catal. Rev. Sci. Eng. 38 (1996) 329.
[30] J. Gao, Y. Qi, W. Yang, X. Guo, S. Li, X. Li, Mater. Chem. Phys. 82 (2003) 602.
[31] A. Trovarelli, Catal. Rev. Sci. Eng. 38 (4) (1996) 439.
[32] S. Melada, M. Signoretto, F. Somma, F. Pinna, G. Cerrato, G. Meligrana, C. Morterra, Catal. Lett. 94 (2004) 193.
[33] M. Signoretto, S. Melada, F. Pinna, S. Polizzi, G. Cerrato, C. Morterra, Micr. Mes. Mater. 81 (2005) 19.
[34] L. Kundakovic, M. Flytzani-Stephanopoulos, J. Catal. 179 (1998) 203.
[35] S.J. Gregg, K.S.W. Sing, Adsorption, Surface Area and Porosity, second ed., Academic Press, New York, 1982, p. 111.
[36] C. Sarzanini, G. Sacchero, F. Pinna, M. Signoretto, G. Cerrato, C. Morterra, J. Mater. Chem. 5 (1995) 353.
[37] B. Lewis, G. von Elbe, Combustion, Flames and Explosion of Gases, Academic Press, New York, 1961.
[38] D.A. Ward, E.I. Ko, J. Catal. 150 (1994) 18.
[39] C. Morterra, G. Cerrato, F. Pinna, M. Signoretto, J. Catal. 157 (1995) 109.
[40] W. Palczewska, in: Z. Paal, P.G. Menon (Eds.), Hydrogen Effects in Catalysis, Dekker, New York, 1988, p. 373.
[41] Z. Karpinski, Adv. Catal. 37 (1990) 45.
[42] G. Fagherazzi, A. Benedetti, S. Polizzi, A. Di Mario, F. Pinna, M. Signoretto, N. Pernicone, Catal. Lett. 32 (1995) 293.
[43] F. Pinna, M. Signoretto, F. Menegazzo, P. Canton, P. Riello, A. Benedetti, N. Pernicone, Stud. Surf. Sci. Catal. 143 (2002) 1011.
[44] D. Andreeva, V. Idakiev, T. Tabakova, L. Ilieva, P. Falaras, A. Bourlinos, A. Travlos, Catal. Today 72 (2002) 51.
[45] T.C. Bissot, US patent 4048096, 1977.
[46] M.S. Chen, D. Kumar, C.W. Yi, D.W. Goodman, Science 310 (2005) 291.
[47] F. Menegazzo, M. Manzoli, A. Chiorino, F. Boccuzzi, T. Tabakova, M. Signoretto, F. Pinna, N. Pernicone, J. Catal. 237 (2006) 431.
[48] F. Menegazzo, F. Pinna, M. Signoretto, V. Trevisan, F. Boccuzzi, A. Chiorino, M. Manzoli, Chem. Sus. Chem. 1 (2008) 320.
[49] F. Boccuzzi, G. Cerrato, F. Pinna, G. Strukul, J. Phys. Chem. B 102 (1998) 5733.
[50] E. Groppo, S. Bertarione, F. Rotunno, G. Agostani, D. Scarano, R. Pellegrini, G. Leofanti, A. Zecchina, C. Lamberti, J. Phys. Chem. C 111 (2007) 7021.
[51] J. Roques, C. Lacaze-Dufaure, C. Mijoule, J. Chem. Theory Comput. 3 (2007) 878.
[52] T. Wei, J. Wang, W. Goodman, J. Phys. Chem. C 111 (2007) 8781, and references therein.
[53] K. Wolter, O. Seiferth, J. Libuda, H. Kuhlenbeck, M. Bäumer, H.-J. Freund, Chem. Phys. Lett. 277 (1997) 513.
[54] A.A. Herzing, A.F. Carley, J.K. Edwards, G.J. Hutchings, C.J. Kiely, Chem. Mater. 20 (2008) 1492.
[55] T. Schalow, B. Brandt, D.E. Starr, M. Laurin, D.S.K. Shaikhutdinov, S. Schauermann, J. Libuda, H.J. Freund, Angew. Chem. Int. Ed. 45 (2006) 3693.
[56] T. Schalow, B. Brandt, D.E. Starr, M. Laurin, D.S.K. Shaikhutdinov, S. Schauermann, J. Libuda, H.J. Freund, Phys. Chem. Chem. Phys. 9 (2007) 1347.
[57] G. Li, J. Edwards, A. Carley, G. Hutchings, Catal. Today 122 (2007) 361.
[58] T. Ishihara, Y. Ohura, S. Yoshida, Y. Hata, H. Nishiguchi, Y. Takita, Appl. Catal. A 291 (2005) 215.
[59] F. Igersheim, H. Mimoun, Nouv. J. Chim. 4 (1980) 711.
[60] J.K. Edwards, B.E. Solsona, P. Landon, A.F. Carley, A. Herzing, C.J. Kiely, G.H. Hutchings, Chem. Mater. 18 (2006) 2690.
[61] D.I. Enache, J.K. Edwards, B.E. Solsona-Espriu, P. Landon, A.F. Carley, A. Herzing, M. Watanabe, C.J. Kiely, D.W. Knight, G.H. Hutchings, Science 311 (2006) 362.